JOURNAL OF CATALYSIS 100, 228–239 (1986)

Effect of Potassium Carbonate on Char Gasification by Carbon Dioxide

PHILIP C. KOENIG,* ROBERT G. SQUIRES, AND NORMAND M. LAURENDEAU

*Coal Research Center, Purdue University, West Lafayette, Indiana 47907; *Amoco Oil Company, P.O. Box 400, Naperville, Illinois 60566*

Received November 6, 1985; revised February 6, 1986

A differential packed-bed reactor has been employed to study the gasification of 7.5 wt% K_2CO_3-catalyzed Saran char in carbon dioxide/carbon monoxide mixtures at a total pressure near 1 atm (101.3 kPa) and temperatures between 922 and 1046 K. The rate data were tested with a model which involves two-site adsorption and subsequent dissociation of CO_2 on the char surface. The results indicate that this model adequately explains the catalyzed gasification data. Moreover, the activation energy for desorption of carbon–oxygen complex is lower for the catalyzed case than for the uncatalyzed case. Adsorption of CO and CO_2 on both catalyzed and uncatalyzed chars was also followed with a volumetric adsorption apparatus at pressures between 1 and 100 kPa and temperatures from 273 to 725 K. The catalyzed char adsorbed an order of magnitude more CO_2 at 560 K than the uncatalyzed char. Subsequent dissociation of CO_2 on the carbon surface does not appear to be catalyzed by potassium. Thus, the catalyst's role is to enhance CO_2 adsorption, thereby creating more oxygen on the surface, and lowering the activation energy for desorption of the resultant carbon–oxygen species.

INTRODUCTION

The catalytic gasification of coal provides a method of achieving higher production rates of medium BTU or synthetic natural gas at lower temperatures than are possible in the absence of a catalyst. Screening studies (*1–3*) have shown that alkali metal salts, in particular the hydroxides and carbonates, are the most effective catalysts. However, many questions remain concerning the catalytic mechanism during gasification.

Most catalytic mechanisms can be classified as either oxygen exchange or electron transfer mechanisms (*4*). In essence, the oxygen exchange mechanism stresses the catalyst's effect on gas adsorption, whereas the electron transfer mechanism stresses its effect on the carbon matrix. Mechanisms and active species for catalyzed gasification have recently been surveyed by Moulijn *et al.* (*5*). They attribute catalytic activity to an increased oxygen transfer from the gas phase to the surface, which results in more carbon–oxygen complex. The subsequent desorption of this carbon–oxygen complex is conjectured to follow the same pathway as for uncatalyzed gasification.

To uncover the catalyst's role during carbon gasification, we have chosen to examine its effect on the known rate expression for uncatalyzed gasification by carbon dioxide. Many experimental studies have been made on the uncatalyzed C–CO_2 gasification reaction. Most investigators have noted that the kinetic data substantiate a rate equation of Langmuir–Hinshelwood form (*6–9*):

$$R = \frac{b_1[CO_2]}{1 + b_2[CO] + b_3[CO_2]} \qquad (1)$$

where R is the intrinsic reactivity (g/m^2s), and the b's represent rate coefficient ratios. The following two-site model was found to agree with Eq. (1) when significant [CO] is present (*10, 11*):

$$CO_2 + 2\,C_f \underset{k_{-1}}{\overset{k_1}{\rightleftharpoons}} C^* \qquad (2)$$

0021-9517/86 $3.00

$$C^* \underset{k_{-2}}{\overset{k_2}{\rightleftharpoons}} C(O) + C(CO) \quad (3)$$

$$C(CO) \underset{k_{-3}}{\overset{k_3}{\rightleftharpoons}} C_f + CO \quad (4)$$

$$C(O) \xrightarrow{k_4} CO, \quad (5)$$

where C_f is a free carbon site, C* is a two-site surface complex, and C(O) and C(CO) are adsorbed species on the carbon surface. For this model, the rate coefficient ratios in Eq. (1) can be expressed as (*10, 11*)

$$b_1 = m_c \frac{k_1 k_2}{k_{-1}} [C_t], \quad b_2 = \frac{k_{-2} k_{-3}}{k_3 k_4}, \quad b_3 = \frac{2 k_1 k_2}{k_{-1} k_4}, \quad (6)$$

where m_c is the mass of a carbon atom and $[C_t]$ is the total number of active sites/m^2. The above two-site model also gives rise to an expression which fits the $[CO_2]^{0.5}$ dependency observed by Turkdogan and Vinters (*12*) and by our group (*10, 11*) for no CO in the inlet gas.

The purpose of this paper is to evaluate the two-site model for gasification of Saran char when catalyzed by potassium carbonate. We will show that this model does indeed fit the catalyzed data. The surface species (C*, C(O), C(CO)) are probably associated with potassium ions (e.g., C* is C*K_x in the catalyzed case, where x indicates an unknown stoichiometry). We will also examine the effect of the catalyst on CO_2 and CO adsorption to gain further insight on the role of the catalyst during gasification.

EXPERIMENTAL METHODS

Materials

The Saran char used in this study is a high-surface-area carbon made by heat-treating Dow Chemical Saran polymer (a copolymer of vinylidene and vinyl chlorides) in nitrogen at 1300 K for 3 h (*13*). Proton Induced X-ray Emission (PIXE) spectroscopy indicated that the most significant impurity was 2300 ppm of chlorine. The major metallic impurity was 25 ppm of niobium. No alkali or alkaline earth metals were detected.

Reagent grade MCB potassium carbonate was used to prepare the catalyzed char samples. The K_2CO_3 was dissolved in deionized water and was added by the incipient wetness technique. The samples used in the kinetic and gas adsorption studies were loaded to a 7.5 wt% loading of potassium carbonate (~0.6 potassium atoms nm^{-2} of char). This loading was determined to be in the linear regime of the rate vs catalyst loading curve. As observed by Wigmans *et al.* (*14*), we found that a minimum loading of catalyst (~2.5 wt%) was needed before the linear regime was entered. In our case, this probably resulted from deactivation of potassium by the residual chlorine in the Saran char, thus forming stable potassium chloride (*15*).

Kinetic Experiments

A differential packed-bed reactor made from 15-mm-i.d. quartz was employed to study the gasification of catalyzed Saran char at a total pressure near 1 atm (101.3 kPa) and temperatures between 922 and 1046 K. The reactor was loaded with between 0.13 and 5.3 g of ~250 μm char particles yielding a bed height between 0.5 and 14.0 cm. The samples were typically pretreated by heating at 1225 K for 2–3 h in flowing argon. During gasification, carbon dioxide, carbon monoxide, and argon at 99.99% purity flowed through the char bed at a total rate between 200 and 1000 cm^3/min (STP). Carbon dioxide was used as the reactant gas, carbon monoxide was added to study its inhibitive effect on gasification, and argon was employed to vary the inlet CO_2 and CO concentrations.

The reaction rates were determined from the amount of CO produced by gasification as measured by an Infrared Industries dual-beam nondispersive infrared analyzer (IR-703D). The mole percentage of CO at the exhaust was typically between 0.6 and

3.4% for experiments with no CO at the inlet, between 14 and 17% for experiments with a constant CO flow at the inlet, and between 4 and 30% for experiments with a varying CO flow at the inlet. The percentage conversion was maintained below 5.0% to ensure differential conditions. The rate was essentially independent of particle size over a 72- to 890-μm range at 1046 K. In addition, the overall activation energy was constant (53.6 ± 1.4 kcal/mol) over a 76 K temperature range between 922 and 998 K for a CO concentration less than 3.4%. These results and a calculated effectiveness factor of unity indicate the absence of intraparticle diffusion limitations (*16*). Moreover, the reaction rate was independent of flow rate for constant space time and flows ≥ 200 cm^3/min (STP) at 1046 K. This result and Mears' criterion (*17*) indicate the absence of interphase diffusion limitations (*16*). The intrinsic reactivities presented in this study were based on the specific surface area at ~10% burn-off using N_2 adsorption (BET isotherm at 77 K). For catalyzed Saran char, CO_2 adsorption does not give reliable surface areas (Dubinin–Raduskevich isotherm at 298 K) because of excessive CO_2 chemisorption.

The dependence of the rate on CO_2 and CO concentrations was determined at temperatures between 997 and 1027 K using a method similar to that of Tyler and Smith (*18*). The carbon dioxide concentration (or carbon monoxide concentration) was step-changed from a typical reference concentration of 40% by volume (17% for CO) to a concentration between 10 and 100% (or a CO concentration between 0 and 27%). After steady state (10–20 min) was established at the new condition, the CO_2 concentration was step-changed back to the reference condition. By interpolating the rate data from two sequential reference concentrations, the rate data from the step-changed $[CO_2]$ and the reference $[CO_2]$ could be compared at a common extent of reaction (i.e., a common pore structure development and surface area). When determined with this method, the influence of $[CO_2]$ on the gasification rate was found to be independent of burn-off.

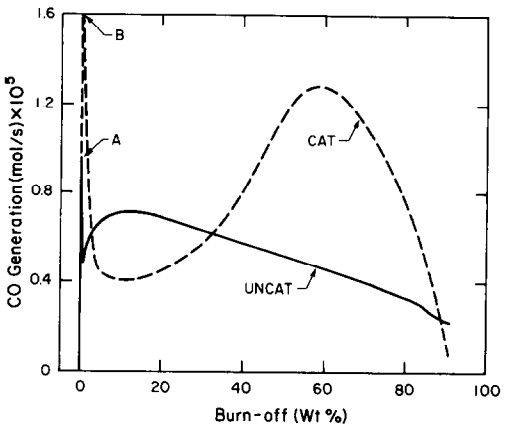

FIG. 1. CO generation as a function of burn-off. CAT—7.5 wt% K_2CO_3-catalyzed Saran char at 990 K, UNCAT—uncatalyzed Saran char at 1204 K. (A) initial CO overshoot for UNCAT, (B) initial CO overshoot for CAT, off-scale.

Unfortunately, the scatter from this method proved to be greater for the catalyzed char than for the uncatalyzed char (*11*). The reason is apparent in Fig. 1 where the CO production for the catalyzed char increases by 100% from 10 to 40% burn-off, while that for the uncatalyzed char drops by only 17% over the same burn-off range. As a consequence of the rapidly changing CO production, the reference reactivities (determined at ~10% burn-off) could vary significantly (±10%) for replicate runs. Consequently, the reference reactivity for a given experiment (e.g., constant [CO] at 997 K) was adjusted within a 10% range of its experimental value to produce the least error when several experiments (e.g., constant [CO], constant $[CO_2]$, constant [CO]/$[CO_2]$, and near-zero [CO] at 997 K) were fit to the two-site model through nonlinear regression analysis.

Adsorption Experiments

For the adsorption experiments, a Micromeretics Accusorb 2100E volumetric adsorption apparatus was employed. The pri-

mary apparatus consisted of a Monel gas manifold (30.2 ml) and an expansion bulb (130.4 ml). The pressure was monitored by a pair of Barocel 1176 electronic manometers. The apparatus was modified by appending a 7-ml quartz cell to the gas manifold using well-insulated Pyrex tubing (7.9 ml). The quartz cell allowed us to employ more severe pretreatments (1250 K) than provided for by the original apparatus. Temperatures were measured with several chromel–alumel thermocouples attached to the outside surfaces of the gas manifold, Pyrex tubing, and quartz cell. Helium was used for all dead-space measurements.

Two primary samples were employed during the adsorption studies—a catalyzed and an uncatalyzed sample which were both activated to 17% burn-off in pure CO_2 at 1085 K. The ratio of the uncatalyzed-to-catalyzed rate on a gram per second basis at this temperature was 6×10^{-3}. A typical pretreatment consisted of heating the sample at low pressure (10^{-4} to 10^{-5} kPa) to 1080 K in 20 min and then immediately cooling the sample to room temperature to minimize the amount of potassium vaporized during the catalyzed experiments. After pretreatment, two types of experiments were performed. In the first kind, the sample was exposed to a known quantity of CO_2 (or CO) at 273–298 K, and adsorption was followed by monitoring the approach to equilibrium via the change in gas pressure. In general, 15–20 min were required to achieve a relatively constant pressure ($\dot{P} < 5 \times 10^{-3}$ kPa/min). The temperature was then increased by 20 to 50 K and the approach to equilibrium was again monitored. This procedure was repeated until a maximum temperature of 725 K was reached. In this way, the amount of CO_2 (or CO) adsorbed was determined as a function of surface temperature. For the second type of experiment, the sample was first heated to the desired temperature (414 to 559 K), after which a known amount of gas was admitted to the sample chamber. Once equilibrium was established ($\dot{P} < 5 \times 10^{-3}$ kPa/min), the gas manifold was closed off from the sample, the pressure was increased, and the sample was again exposed. In this manner, an adsorption isotherm was produced.

Whereas only physisorption (heat of adsorption ~5 kcal/mol) took place during CO_2 adsorption on uncatalyzed char, both physisorption and chemisorption (heat of adsorption >10 kcal/mol) occurred during CO_2 adsorption on the catalyzed samples. Since CO_2 chemisorption was partially reversible, the usual way of separating physisorption from chemisorption (i.e., adsorb gas on surface, evacuate at adsorption temperature, and then perform second adsorption) was not applicable. Consequently, to correct for physisorption on the catalyzed samples, we used a two-site Langmuir isotherm (discussed subsequently) to calculate the amount of physisorption that would have occurred on an uncatalyzed sample of equal surface area (BET isotherm with N_2 at 77 K) at the temperature and pressure of each point in the catalyzed adsorption experiment. In this way, we could examine the amount of CO_2 chemisorbed on the catalyzed sample as a function of temperature and pressure. The CO_2 chemisorbed varied from 48% of the total CO_2 adsorbed at 273 K to 96% at 720 K.

RESULTS AND DISCUSSION

Kinetic Model for Catalyzed Gasification

Equation (1) has previously been found to fit uncatalyzed gasification for significant [CO] using Saran char (*11*) and other carbons (*10, 14, 19*). Inverting Eq. (1) gives

$$\frac{1}{R} = \frac{b_3}{b_1} + \frac{b_2}{b_1}\frac{[CO]}{[CO_2]} + \frac{1}{b_1}\frac{1}{[CO_2]}. \quad (7)$$

Thus, when [CO] is significant the following relationships should exist at constant temperature if the two-site model holds:

1. $1/R$ vs $1/[CO_2]$ should be linear for constant [CO] with a positive intercept;

2. $1/R$ vs $1/[CO_2]$ should be linear for constant $[CO]/[CO_2]$ with a positive intercept;

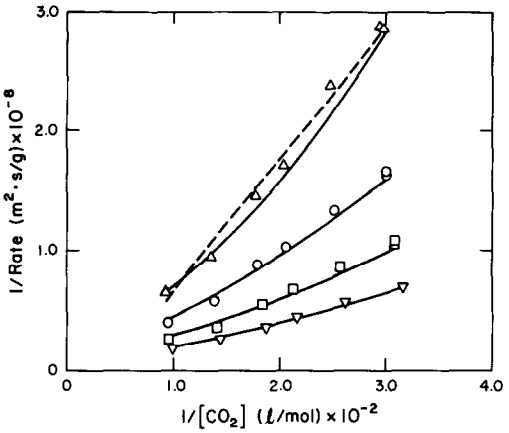

FIG. 2. Test of Eqs. (7) (---) and (9) (———) for 7.5 wt% K_2CO_3-catalyzed Saran char with [CO] ~ 15 kPa (1.5×10^{-3} mol/liter). (△) 997 K, (○) 1006 K, (□) 1017 K, (▽) 1027 K.

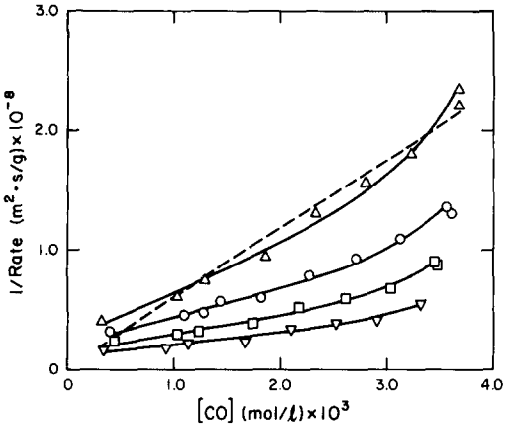

FIG. 4. Test of Eqs. (7) (---) and (9) (———) for 7.5 wt% K_2CO_3-catalyzed Saran char with [CO_2] ~ 60 kPa (6.0×10^{-3} mol/liter). (△) 997 K, (○) 1006 K, (□) 1017 K, (▽) 1027 K.

3. $1/R$ vs [CO] should be linear for constant [CO_2] with a positive intercept.

Catalyzed data for these relationships are plotted in Figs. 2–4. Examination of these plots indicates that the above relationships do not hold in the presence of catalyst. For example, the plots of $1/R$ vs $1/[CO_2]$ for [CO] ~ 15 kPa in Fig. 2 were fit by linear regression analysis and yielded good straight lines (e.g., dashed line for 997 K data). However, these lines showed statistically significant negative intercepts which are physically impossible since rate coefficients cannot be negative. The data in Fig. 4 also display a definite concave-upward curvature rather than the expected straight line (e.g., dashed line for 997 K data). Apparently, the catalyst influences the model in such a way that the above relationships for significant [CO] do not hold at these temperatures.

Interestingly, linear regression of the data for no CO in the inlet (Fig. 5) still indicates a $[CO_2]^{0.5}$ dependency and yields the

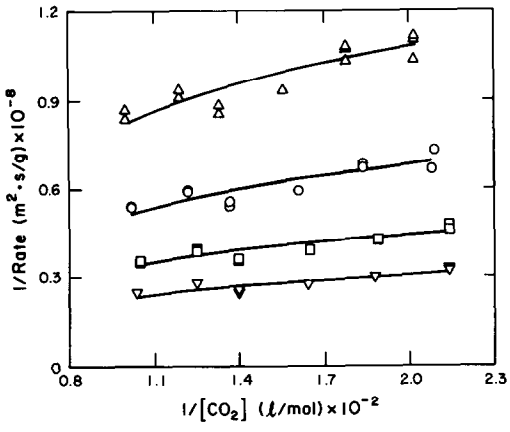

FIG. 3. Test of Eqs. (7) and (9) for 7.5 wt% K_2CO_3-catalyzed Saran char with [CO]/[CO_2] ~ 0.25. (△) 997 K, (○) 1006 K, (□) 1017 K, (▽) 1027 K.

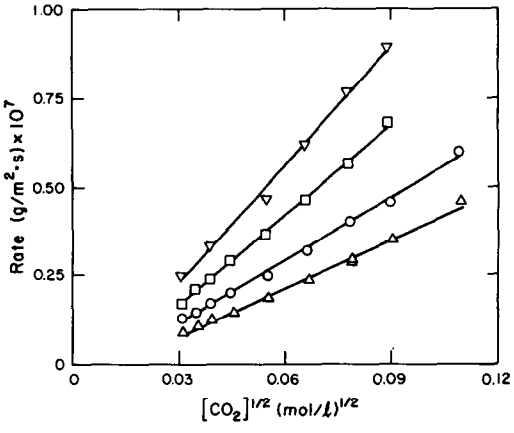

FIG. 5. Test of Eq. (9) for 7.5 wt% K_2CO_3-catalyzed Saran char with [CO] ~ 1 kPa (1.0×10^{-4} mol/liter). (△) 997 K, (○) 1006 K, (□) 1017 K, (▽) 1027 K.

anticipated negative intercepts as for the noncatalytic case (*10, 11*). Thus the near-zero [CO] results suggest that the two-site model still holds. Since significant CO concentrations are needed to cause a departure from the expected results, we attempted to modify the two-site model by adding steps involving CO adsorption and decomposition. Equations were developed which fit the CO data, but once again, the results gave negative rate coefficients. Therefore, these models were discarded.

The fundamental assumption made in reducing the two-site model to Eq. (1) was that at the high temperatures associated with uncatalyzed gasification, significant [CO] reduces the amount of C(O) on the surface to the point where $[C_t] \gg [C(O)]$ (*10, 11*). Several results indicate that this assumption is invalid for catalyzed gasification:

1. Using Auger electron spectroscopy (AES), Kelemen *et al.* (*20*) observed a higher O/C ratio for KOH-catalyzed glassy carbon as compared to the uncatalyzed carbon.

2. From mass balance calculations, Yokoyama *et al.* (*21*) noted that the amount of oxygen on a 0.9 wt% K_2CO_3-catalyzed activated carbon is 5 to 10 times the quantity on a uncatalyzed carbon at 973 K, even in the presence of significant [CO].

3. In our experiments, the CO overshoot during the initial exposure of Ar-pretreated char samples was 40–50 times larger for a 7.5 wt% K_2CO_3-catalyzed Saran char than for the uncatalyzed char at 1085 K. The overshoot indicates the amount of atomic oxygen which is dissociated from the CO_2, and thus provides a rough measure of the quantity of oxygen on the surface at the beginning of gasification.

Even though the above results do not distinguish between oxygen associated with the potassium and oxygen chemisorbed on carbon, one can reasonably presume that some of this oxygen produces more C(O) (or C(O)K if potassium is associated with the species) on the surface. As a result of the increased [C(O)], the following equation derived in our previous work (*10*) must be solved for [C(O)]:

$$[C(O)]^2\left[\frac{k_2k_{-2}(k_4 - k_{-3}[CO])}{(k_2 + k_{-1})k_3} + \frac{k_1k_2[CO_2]}{(k_2 + k_{-1})} - \frac{k_{-2}(k_4 - k_{-3}[CO])}{k_3}\right] + [C(O)][C_t] \times\left[\frac{k_2k_{-2}k_{-3}[CO]}{(k_2 + k_{-1})k_3} - \frac{2k_1k_2[CO_2]}{(k_2 + k_{-1})} - \frac{k_{-2}k_{-3}[CO]}{k_3} - k_4\right] + [C_t]^2\left[\frac{k_1k_2[CO_2]}{(k_2 + k_{-1})}\right] = 0. \quad (8)$$

Following our previous work, we will still assume that $k_{-1} \gg k_2$ (i.e., the CO_2 desorption rate is much faster than the CO_2 decomposition rate). The quadratic equation can then be used to solve for the intrinsic reactivity since $R = m_c k_4[C(O)]$:

$$R = \frac{(-a_1[CO] - a_2[CO_2] - a_3 + \sqrt{a_4[CO_2] + a_5 + a_6[CO] + a_7[CO]^2})}{a_8 - a_9[CO] - a_{10}[CO_2]}, \quad (9)$$

where the a's represent the catalyzed rate coefficient ratios:

$$a_1 = m_c\frac{k_{-2}k_{-3}}{k_3}[C_t],\ a_2 = m_c\frac{2k_1k_2}{k_{-1}}[C_t],$$

$$a_3 = m_ck_4[C_t],$$

$$a_4 = m_c^2\frac{4k_1k_2k_4}{k_{-1}}\left[1 + \frac{k_{-2}}{k_3}\right][C_t]^2,$$

$$a_5 = m_c^2k_4^2[C_t]^2,\ a_6 = m_c^2\frac{2k_4k_{-2}k_{-3}}{k_3}[C_t]^2,$$

$$a_7 = m_c^2\left[\frac{k_{-2}k_{-3}}{k_3}\right]^2[C_t]^2,\ a_8 = \frac{2k_{-2}}{k_3},$$

$$a_9 = \frac{2k_{-2}k_{-3}}{k_3k_4},\ a_{10} = \frac{2k_1k_2}{k_{-1}k_4}. \quad (10)$$

Preliminary nonlinear regression analysis of the data using Eq. (9) indicated that a_2 and a_{10} were negligible in comparison to the other terms. The ~200 K lower temperatures used here, as well as the catalyst's interaction with CO_2 and CO, could explain why these terms are negligible in the catalyzed case but not for the uncatalyzed case. Using a nonlinear regression analysis based

TABLE 1

Parameter Values for Eq. (9) as a Function of Temperature

Parameter[a]	997 K	1006 K	1017 K	1027 K
$a_1 \times 10^3$	2.42	4.01	6.37	7.11
$a_3 \times 10^7$	5.30	6.75	9.08	11.6
$a_4 \times 10^9$	0.40	1.46	4.78	11.2
$a_5 \times 10^{13}$	3.02	4.83	8.30	13.7
$a_6 \times 10^9$	2.46	5.64	12.7	15.0
$a_7 \times 10^5$	0.57	1.53	3.86	4.73
$a_8 \times 10^{-1}$	3.27	5.20	7.08	8.63
$a_9 \times 10^{-3}$	5.23	9.90	13.9	13.8

[a] a's are defined in Eq. (10), with the following units: a_1 (g liter/m^{2}s mol), a_3 (g/m^{2}s), a_4 (g^2 liter/m^{4}s^2 mol), a_5 (g^2/m^{4}s^2), a_6 (g^2 liter/m^{4}s^2 mol), a_7 (g^2 liter^2/m^{4}s^2 mol^2), a_8 (dimensionless), a_9 (liter/mol).

on Marquardt's method, the resulting eight-parameter equation was employed to simultaneously fit the constant [CO], constant [CO_2], constant [CO]/[CO_2], and near-zero [CO] data at each temperature (997, 1006, 1017, 1027 K).

Closer examination of Eq. (10) reveals several relationships that should exist among the parameters. For example, $m_c k_4[C_t]$ can be calculated from a_3 and a_5 ($a_3 = a_5^{0.5}$). These values can be averaged and used to calculate values of $m_c k_{-2} k_{-3}[C_t]/k_3$ from a_6 and a_9, which can be compared to those directly calculated from a_1 and a_7 ($a_1 = a_7^{0.5}$). The agreement between the $m_c k_4[C_t]$ values and among the $m_c k_{-2} k_{-3}[C_t]/k_3$ values calculated from a_1, a_6, and a_7 did not depend on the initial guesses for these parameters. However, agreement of the $m_c k_{-2} k_{-3}[C_t]/k_3$ value determined from a_9 with the other three values was found to be sensitive to the initial guess. To arrive at a final set of parameter values, the average value of $m_c k_4[C_t]$ (from a_3 and a_5) for each temperature was constrained to lie on an Arrhenius plot with an activation energy of 53.6 kcal/mol (determination of this value is discussed subsequently). The sum-of-squares of the difference between the value of $m_c k_{-2} k_{-3}[C_t]/k_3$ calculated from a_9 and that averaged from a_1, a_6, and a_7 at each temperature was then minimized. The final set of parameters appears in Table 1; the fits appear in Figs. 2–5. The good agreement between the $m_c k_4[C_t]$ values and among the $m_c k_{-2} k_{-3}[C_t]/k_3$ values for the parameters in Table 1 is demonstrated in Table 2. This agreement supports the two-site model.

Definite statements concerning the catalyst's effect on the individual rate coefficients are precluded by the narrow temperature range (~30 K) over which we were forced to operate to maintain differential conditions. However, information may still be gleaned by comparing the overall activation energies for catalyzed and uncatalyzed gasification. Since $R = m_c k_4[C(O)]$, the overall activation energy should be equal to the activation energy for k_4 if [C(O)] is independent of temperature. For Saran char with near-zero [CO], the overall activation energy was 80.9 ± 2.2 kcal/mol from 1131 to 1225 K for the uncatalyzed case (16), and 53.6 ± 1.4 kcal/mol from 922 to 998 K for the catalyzed case. The small standard deviations in these values suggest that [C(O)] is relatively constant for these narrow temperature ranges, since some curvature (and thus larger errors) in the Arrhenius plots would be expected if [C(O)] changed significantly. Thus, we may conclude that the activation energy for k_4 (E_4) is smaller for catalyzed gasification, indicating a weakening of carbon–carbon bonds in this case. Kele-

TABLE 2

Comparison of $m_c k_4[C_t] \times 10^7$ (g/m^{2}s) and $m_c k_{-2} k_{-3}[C_t]/k_3 \times 10^3$ (g liter/m^{2}s mol) Values as Calculated from Table 1

$m_c k_4[C_t]$			$m_c k_{-2} k_{-3}[C_t]/k_3$[a]			
Temp. (K)	a_3	$a_5^{0.5}$	a_1	$a_7^{0.5}$	$a_6/2\bar{a}$	$a_9\bar{a}/2$
997	5.30	5.50	2.42	2.39	2.28	1.41
1006	6.75	6.95	4.01	3.91	4.12	3.39
1017	9.08	9.11	6.37	6.21	6.98	6.32
1027	11.6	11.7	7.11	6.88	6.44	8.04

[a] $\bar{a} = (a_3 + a_5^{0.5})/2$.

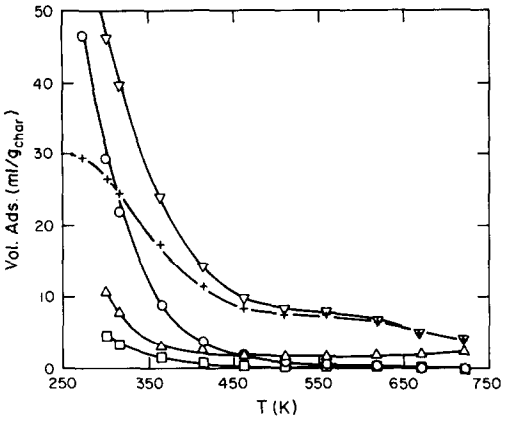

FIG. 6. CO_2 and CO adsorption on an uncatalyzed Saran char and a 7.5 wt% K_2CO_3-catalyzed Saran char activated to 17% burn-off. Symbols: (▽) total CO_2 adsorption on catalyzed char, where vol. ads. at 273 K ~61 ml/g (P_m = 53 kPa); (+) CO_2 chemisorption on catalyzed char (P_m = 53 kPa); (○) total CO_2 adsorption on uncatalyzed char (P_m = 53 kPa); (△) total CO adsorption on catalyzed char (P_m = 40 kPa); (□) total CO adsorption on uncatalyzed char (P_m = 40 kPa); where P_m is the initial manifold pressure before adsorption.

men and Freund (*22*) and Nayak and Jenkins (*23*) have noted that an increase in [C(O)] can reduce E_4. Hence, the lower E_4 (i.e., weaker C–C bonds) observed here can be attributed to an increased [C(O)] during catalyzed gasification. This result is consistent with our earlier observation where we found that the two-site model fits catalyzed data for high [CO] only if [C(O)]/[C_t] is significant; for uncatalyzed data, [C(O)]/[C_t] $\ll$ 1 at high [CO] (*10*, *11*).

The ability of the two-site model to provide physically significant parameters and the good agreement among these parameters support this model for catalyzed gasification. Although the exact structures for the surfaces species (C*, C(O), and C(CO)) are uncertain, they are probably associated with surface potassium ions (e.g., C* is C*K_x in the catalyzed case, where x indicates unknown stoichiometry) (*5*). Results to be discussed subsequently indicate that the catalyst affects CO_2 and CO adsorption (Reactions (2) and (4)), but not CO_2 dissociation (Reaction (3)). The primary effect of the catalyst can be attributed to the catalyst's proficiency in creating more C(O) via enhanced CO_2 adsorption. The increased [C(O)] lowers the activation energy for desorption of this complex (Reaction (5)).

Effect of Catalyst on Gas Adsorption

Figure 6 illustrates the adsorption of CO_2 and CO as a function of temperature on both catalyzed and uncatalyzed chars activated to 17% burn-off. The amount of CO_2 adsorbed on the uncatalyzed char (circles) reaches 46 ml/g at 273 K for a starting manifold pressure of 53 kPa. The amount adsorbed quickly decreases to ~8% of this value by 415 K. CO adsorption on the uncatalyzed char (squares) is much smaller and drops to less than 1 ml/g near 400 K.

As mentioned earlier, both physisorption and chemisorption of CO_2 take place on the catalyzed char (inverted triangles). Subtracting the physisorption contribution (discussed previously) yields the amount of CO_2 chemisorbed on the surface (crosses). The amount of chemisorption approaches saturation at 273 K for a starting manifold pressure of 53 kPa. The amount of CO_2 on the surface after equilibration at this temperature (equilibrium pressure = 13 kPa) represents 0.92 CO_2 molecules per potassium atom present. As the temperature increases, the quantity of CO_2 decreases until it plateaus at temperatures between 460 and 560 K. The amount of CO_2 on the surface after equilibration at this temperature (equilibrium pressure ~34 kPa) corresponds to 0.24 CO_2 molecules per K atom, and agrees with the values reported by Ratcliffe and Vaughn (*24*) using CO_2 adsorption at 573 K on Spherocarb and by Mims *et al.* (*25*) employing ^{13}C NMR on methylated Spherocarb.

CO adsorption on the catalyzed surface (triangles) is greater than on the uncatalyzed surface for the same starting manifold pressure, but it is still considerably smaller than CO_2 adsorption. CO adsorption appears to increase at $T > 450$ K; however, CO disproportionation into CO_2 and C occurs as evidenced by significant CO_2 in the

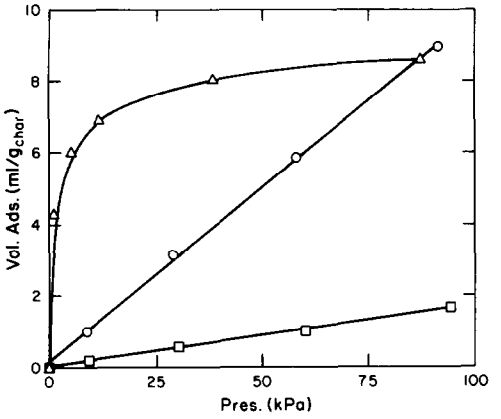

FIG. 7. CO_2 adsorption isotherms on a 7.5 wt% K_2CO_3-catalyzed Saran char at 559 K (△) and an uncatalyzed Saran char at 414 K (○) and 559 K (□). For the uncatalyzed case, the isotherm represents physisorption; for the catalyzed case, the isotherm represents chemisorption.

gas manifold after 50 h at 688 K. The CO_2 formed by disproportionation adsorbs on the surface and causes the apparent increase in CO adsorption. Yokoyama *et al.* (*21*) have also observed CO disproportionation over potassium-catalyzed activated carbon. They additionally noted that some CO_2 is formed because CO can strip oxygen off the surface. The disproportionation of CO is catalyzed by the potassium; the amount of CO_2 formed on the uncatalyzed char after 50 h at 688 K was only 7% of the quantity formed over the catalyzed sample.

Adsorption isotherms for CO_2 on catalyzed and uncatalyzed Saran char appear in Fig. 7. The linear plots for the uncatalyzed char indicate that the data is in the low coverage regime of a Langmuir isotherm. This result can be anticipated since the quantity of CO_2 on the surface at these pressures and temperatures is less than 5% of the total allowed by physisorption. Since the data are in the low coverage regime, single-site and two-site Langmuir isotherms fit equally well. In contrast to CO_2 physisorption, CO_2 chemisorption at 559 K on the catalyzed char displays extreme curvature and approaches saturation at higher pressures. The chemisorption data were fit with both a single-site and a two-site Langmuir isotherm. The residual sum of squares for the two-site fit was 30 times smaller than that for the single-site fit; the fit for the two-site model is shown in Fig. 7. This result supports Reaction (2), which involves the two-site adsorption of CO_2 to form a complex of unknown structure on the surface (e.g., C^*K_x).

Based on the above, the following two-site Langmuir model was employed to calculate equilibrium constants for CO_2 adsorption on both the uncatalyzed and catalyzed chars using the data in Fig. 6:

$$K = \frac{1}{P}\frac{V/V^*}{\left[1 - \frac{V}{V^*}\right]^2}, \qquad (11)$$

where K is the equilibrium constant in kPa^{-1}, P is the pressure in kPa, $V(P,T)$ is the volume adsorbed in ml/g_{char} and $V^*(P, T)$ is the saturation coverage in ml/g_{char}. For the uncatalyzed data a saturation coverage corresponding to the total surface area at 17% burn-off was used (assuming 16 ml (STP) CO_2 adsorbed/m^2 based on 1 molecule CO_2/0.253 nm^2; (*26*)). As shown in Fig. 8, the calculated equilibrium constants are linear on an Arrhenius plot for temperatures less than 560 K ($1/T > 1.8 \times 10^{-3}$ K^{-1}). The heat of adsorption calculated for this region (273–560 K) is 5.78 ± 0.09 kcal/

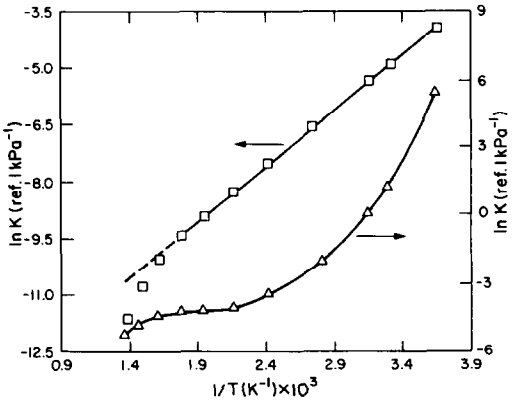

FIG. 8. Arrhenius plot of CO_2 physisorption on an uncatalyzed Saran char (□) and CO_2 chemisorption on a 7.5 wt% K_2CO_3-catalyzed Saran char (△).

mol. At temperatures greater than 560 K ($1/T < 1.8 \times 10^{-3}$ K^{-1}), the amount of CO_2 on the surface is less than the quantity calculated by extrapolation from the linear region. Although the amount of CO_2 on the surface is small at these high temperatures, the downward curvature above 560 K was reproducible. Using X-ray and ultraviolet photoemission spectroscopies, Kelemen and Freund (*22*) observed CO_2 dissociation on a clean glassy carbon to give gaseous CO and surface C(O) at 573 K. This dissociation of CO_2 on the surface could account for the observed departure from linearity at 560 K.

An Arrhenius plot for the catalyzed char is also shown in Fig. 8 for a saturation coverage of 30 ml/g. The plot displays concave-upward curvature at large $1/T$ (small T), which levels off at $1/T$ between 1.8×10^{-3} and 2.2×10^{-3} K^{-1}. This plateau suggests the formation of a relatively stable complex containing CO_2 on the catalyzed surface at 460–560 K. At temperatures greater than 560 K ($1/T < 1.8 \times 10^{-3}$ K^{-1}) the amount of CO_2 on the surface starts to decrease. After exposing the catalyzed sample to 65 kPa of CO_2 at 688 K for 65 h, the manifold contained ~2.5% CO. This result suggests that the drop in adsorbed CO_2 for $T > 560$ K is partially due to CO_2 dissociation. Using isotope tracer experiments for a potassium carbonate-catalyzed carbon black, Saber *et al.* (*27*) found that oxygen exchange between gaseous and surface CO_2 became appreciable at temperatures near 600 K, which also indicates the occurrence of CO_2 dissociation on the surface.

The adsorption results clearly show that CO_2 and CO adsorption on a catalyzed char are considerably different than that for an uncatalyzed char. The catalyzed char adsorbs approximately eight times as much CO_2 than the uncatalyzed char at 500 K. Moreover, CO_2 on *both* the uncatalyzed and catalyzed surfaces dissociates forming gas-phase CO and surface C(O) at temperatures greater than 560 K. This result suggests that, although the thermodynamics and kinetics of CO_2 adsorption are different for the uncatalyzed and potassium-catalyzed char (i.e., C* is formed on the uncatalyzed surface; C^*K_x on the catalyzed surface), the subsequent dissociation of CO_2 is not catalyzed by potassium (i.e., k_2 is approximately the same during uncatalyzed and catalyzed gasification). Thus, the enhanced oxygen exchange rate reported by Mims and Pabst (*28*) for potassium-catalyzed Spherocarb at 588 K results from an increased quantity of surface CO_2 ($[C^*K_x] > [C^*]$ at 588 K), with which gas-phase CO_2 can exchange oxygen. The major effect of the catalyst is to augment the CO_2 adsorption rate, thereby creating more C(O) on the catalyzed surface during the subsequent dissociation of the CO_2.

Effect of Catalyst on Rate vs Burn-off Curve

The CO generation rate on a mol per second basis is shown in Fig. 1 as a function of burn-off for an uncatalyzed sample at 1204 K and for a 7.5 wt% K_2CO_3-catalyzed sample at 990 K. Similar behavior was observed at all other temperatures: 922 to 1046 K for catalyzed samples, and 1131 to 1229 K for uncatalyzed samples. Both samples initially contained 0.64 g of Saran char. Exposure of the Ar-pretreated samples to CO_2 resulted in a CO overshoot for both the uncatalyzed char (point A in Fig. 1) and the catalyzed char (point B: the overshoot was off-scale in this case). The uncatalyzed rate reached a maximum in the 5–20% burn-off range, followed by a gradual decrease to 91% burn-off. This decline parallels the observed reduction in available surface area for uncatalyzed Saran char at higher burn-offs (*13*).

We expected the catalyzed rate (on a mol per second basis) to remain constant over a majority of the burn-off range since the amount of active catalyst on a pure carbon decreases only slightly until high burn-offs (*24*). That this is not the case is clearly evident in Fig. 1, where the catalyzed rate increases threefold from 10 to 60% burn-off.

Wigmans *et al.* (*29*) have reported similar results for a purified activated carbon. As discussed earlier, the loading used in these experiments was in the linear regime of the rate vs catalyst loading curve; i.e., saturation coverage of the surface has not been reached. Furthermore, the total surface area (BET isotherm with N_2 at 77 K) available to the catalyst stays relatively constant over the 10 to 60% burn-off range (e.g., for an initial char weight of 0.64 g, the surface area is 550 m^2 at 17% burn-off and 531 m^2 at 40% burn-off). Consequently, the observed threefold rate enhancement cannot be attributed to a further spreading of the catalyst over the char surface with increasing burn-off.

An examination of the parameters which directly control the measured CO production can help explain the sharp growth in the catalyzed rate. After the initial unsteady state overshoot, a pseudo-steady-state condition is reached in which the CO generation rate is equal to $2k_4$[C(O)], where k_4 is the rate coefficient for desorption of the C(O) complex. The factor of two results from the dissociation of CO_2 to also give CO under pseudo-steady-state conditions. Therefore, for the rate to buildup, [C(O)] must increase if k_4 remains relatively constant during gasification. This suggests that the rate of CO_2 dissociation is slightly larger than the rate of C(O) desorption at pseudo-steady state, implying that the catalyst must be sufficiently mobile to create C(O) and then migrate to a new unoxidized carbon site before the C(O) with which it was previously associated desorbs. The mobility of a potassium species on the surface is well documented (*30*). The sharp drop at high burn-offs is probably the consequence of the catalyst losing intimate contact with the reducing amount of carbon. Inactive potassium containing particles have been observed to form during CO_2 gasification of K_2CO_3-catalyzed graphite (*30*).

CONCLUSIONS

The principal results obtained in this investigation can be summarized as follows.

1. The same two-site model, which successfully fit uncatalyzed gasification data (*10, 11*), also explains K_2CO_3-catalyzed gasification data. The surface species (C*, C(O), C(CO) are probably associated with potassium ions. In contrast to the uncatalyzed case, the amount of C(O) on the surface is not negligible in the presence of significant [CO] (~15 kPa). A two-site Langmuir isotherm also provides the best fit to the CO_2 adsorption data, thus supporting the efficacy of the two-site model.

2. Activation energies for k_4 (E_4), derived from the overall activation energies for gasification of catalyzed and uncatalyzed Saran char, are smaller for catalyzed gasification, indicating a weakening of carbon–carbon bonds in this case. A smaller E_4 implies that [C(O)] is greater during catalyzed gasification, which is consistent with the first conclusion.

3. Gas adsorption experiments indicate that potassium is able to form a complex with CO_2 which is stable up to 560 K. The amount of CO_2 adsorption at this temperature is an order of magnitude higher on the catalyzed surface than on the uncatalyzed surface. CO_2 on both the uncatalyzed and catalyzed surface dissociates at temperatures greater than 560 K, suggesting that the dissociation is not catalyzed by potassium.

4. For uncatalyzed gasification, CO generation gradually tapers off after 20% burn-off due to a reduction in available surface area. During catalyzed gasification, a sharp increase in CO production occur in the 10–60% burn-off range. This enlargement can be accounted for by a buildup of C(O) on the catalyzed surface.

Collectively, our results indicate that [C(O)] is greater for K_2CO_3-catalyzed gasification than for uncatalyzed gasification. The primary effect of the catalyst is to increase the amount of oxygen transferred from the gas phase to the carbon surface by augmenting CO_2 adsorption. The resultant increase in [C(O)] weakens carbon–carbon bonds, suggesting an enhanced electron transfer from the carbon matrix to the sur-

face C(O) species. Thus, the catalyst enhances both oxygen and electron transfer; however, its effect on electron transfer is through increased [C(O)], and not via the formation of a potassium–carbon intercalation compound. The rate enlargement during catalyzed gasification can be attributed to a combination of increased [C(O)] and a smaller activation energy for desorption of C(O).

ACKNOWLEDGMENTS

This study was supported by a grant from Conoco, Inc. through the Coal Research Center at Purdue University. We appreciate the helpful comments of Professor R. P. Andres, Professor W. N. Delgass, Professor C. G. Takoudis, and other members of the catalysis group in the Chemical Engineering Department at Purdue University. In addition, we are thankful to B. J. Waters for his assistance with this work.

REFERENCES

1. Veraa, M. J., and Bell. A. T., *Fuel* **57,** 194 (1978).
2. Wilkes, K. A., Gardner, N. C., and Angus, J. C., *Amer. Chem. Soc. Div. Fuel Chem. Prepr. Pap.* **20**(3), 52 (1975).
3. Haynes, W. P., Gasior, S. J., and Forney, A. J., *Amer. Chem. Soc. Div. Fuel Chem. Prepr. Pap.* **131,** 179 (1974).
4. Walker, P. L., Jr., Shelef, M., and Anderson, R. A., *in* "Chemistry and Physics of Carbon" (P. L. Walker, Jr., Ed.), Vol. 4, p. 287. Dekker, New York, 1968.
5. Moulijn, J. A., Cerfontain, M. B., and Kapteijn, F., *Fuel* **63,** 1043 (1984).
6. Walker, P. L., Jr., Rusinko, F., Jr., and Austin, L. G., *in* "Advances in Catalysis" (D. D. Eley, P. W. Selwood, and P. B. Weisz, Eds.), Vol. 11, p. 133. Academic Press, New York, 1959.
7. Gadsby, J., Long, F. J., Sleightholm, P., and Sykes, K. W., *Proc. R. Soc. London Ser. A* **103,** 357 (1948).
8. Mentser, M., and Ergun, S., "A Study of the Carbon Dioxide–Carbon Reaction by Oxygen Exchange." U.S. Bureau of Mines Bulletin 664, 1973.
9. Laurendeau, N. M., *Prog. Energy Combust. Sci.* **4,** 221 (1978).
10. Koenig, P. C., Squires, R. G., and Laurendeau, N. M., *Carbon* **23,** 531 (1985).
11. Koenig, P. C., Squires, R. G., and Laurendeau, N. M., *Fuel* **65,** 412 (1986).
12. Turkdogan, E. T., and Vinters, J. V., *Carbon* **7,** 101 (1969).
13. Waters, B. J., M.S. thesis. Purdue University, 1985.
14. Wigmans, T., Hoogland, A., Tromp, P., and Moulijn, J. A., *Carbon* **21**(1), 13 (1983).
15. Mims, C. A., and Pabst, J. K., *Amer. Chem. Soc. Div. Fuel Chem. Prepr. Pap.* **25**(3), 258 (1980).
16. Koenig, P. C., Ph.D. thesis. Purdue University, 1985.
17. Mears, D. E., *J. Catal.* **20,** 127 (1971).
18. Tyler, R. J., and Smith, J. W., *Fuel* **54,** 100 (1975).
19. Strange, J. F., and Walker, P. L., Jr., *Carbon* **14,** 345 (1976).
20. Kelemen, S. R., Freund, H., and Mims, C. A., *Amer. Chem. Soc. Div. Fuel Chem. Prepr. Pap.* **30**(1), 349 (1985).
21. Yokoyama, S., Miyahara, K., Tanaka, K., Takakuwa, I., and Tashiro, J., *Fuel* **58,** 510 (1979).
22. Kelemen, S. R., and Freund, H., *Amer. Chem. Soc. Div. Fuel Chem. Prepr. Pap.* **30**(1), 286 (1985).
23. Nayak, R. V., and Jenkins, R. G., *Amer. Chem. Soc. Div. Fuel Chem. Prepr. Pap.* **29**(2), 172 (1984).
24. Ratcliffe, C. T., and Vaughn, S. N., *Amer. Chem. Soc. Div. Fuel Chem. Prepr. Pap.* **30**(1), 304 (1985).
25. Mims, C. A., Rose, K. D., Melchior, M. T., and Pabst, J. K., *J. Amer. Chem. Soc.* **104,** 886 (1982).
26. Taylor, R. L., Ph.D. thesis. The Pennsylvania State University, 1982.
27. Saber, J. M., Falconer, J. L., and Brown, L. F., *J. Catal.* **90,** 65 (1984).
28. Mims, C. A. and Pabst, J. K., *Amer. Chem. Soc. Div. Fuel Chem. Prepr. Pap.* **25**(3), 263 (1980).
29. Wigmans, T., Elfring, M., and Moulijn, J. A., *Carbon* **21**(1), 1 (1983).
30. Mims, C. A., Chludzinski, J. J., Jr., Pabst, J. K., and Baker, R. T. K., *J. Catal.* **88,** 97 (1984).